On the origin of multiple BSRs in the Danube deep-sea fan, Black Sea

Timo Zander[1], Matthias Haeckel[1], Christian Berndt[1], Wu-Cheng Chi[2], Ingo Klaucke[1], Joerg Bialas[1], Dirk Klaeschen[1], Stephanie Koch[1], Orhan Atgın[3]

[1]Geomar Helmholtz Centre for Ocean Research Kiel, Wischhofstraße 1-3, 24148 Kiel, Germany

[2]Institute of Earth Sciences, Academia Sinica, No. 128, Academia Road, Sec 2, Nangang Dist., Taipei, Taiwan

[3]Institute of Marine Sciences and Technology, Dokuz Eylül University, Bakü Street, 35340 Inciralti, Izmir, Turkey

Corresponding Author: Timo Zander, tzander@geomar.de

Keywords: Black Sea, bottom simulating reflection (BSR), multiple BSRs, heat flow, gas hydrates

Abstract

High-resolution 2D seismic data reveal the character and distribution of up to four stacked bottom simulating reflectors (BSR) within the channel-levee systems of the Danube deep-sea fan. The theoretical base of the gas hydrate stability zone (GHSZ) calculated from regional geothermal gradients and salinity data is in agreement with the shallowest BSR. For the deeper BSRs, BSR formation due to overpressure compartments can be excluded because the necessary gas column would exceed the vertical distance between two overlying BSRs. We show instead that the deeper BSRs are likely paleo BSRs caused by a change in pressure and temperature conditions during different limnic phases of the Black Sea. This is supported by the observation that the BSRs correspond to paleo seafloor horizons located in a layer between a buried channel-levee system and the levee deposits of the Danube channel. The good match of the observed BSRs and the BSRs predicted from deposition of these sediment layers indicates that the multiple BSRs reflect stages of stable sealevel lowstands possibly during glacial times. The observation of sharp BSRs several 10,000 of years but possibly up to 300,000 years after they have left the GHSZ demonstrates that either hydrate dissociation does not take place within this time frame or that only small amounts of gas are released that can be transported by diffusion. The gas underneath the previous GHSZ does not start to migrate for several thousands of years.

1. Introduction

A bottom simulating reflector (BSR) in seismic reflection data is a common indicator for gas hydrates in marine sediments. It is a distinct reflector that is caused by the negative impedance contrast between high-velocity gas-hydrate-bearing sediments above and low-velocity gas-bearing sediments below (Hyndman and Davis, 1992). It follows the base of the gas hydrate stability field and is consequently sub-parallel to the seafloor, frequently crosscutting reflectors and stratigraphic sequences. On many occasions, the BSR is patchy and discontinuous, depending on the geology, as gas is more likely trapped in highly permeable layers bounded by impermeable layers (Judd and Hovland, 2007). The gas hydrate stability field is controlled by pressure, temperature (bottom-water temperature and geothermal gradient in the sedimentary column), salinity, and gas composition (Shipley et al., 1979). In the marine environment, gas hydrates primarily consist of methane and dominantly form in crystallographic structure I (e.g. Sloan, 1998).

Studies showed that free-gas concentrations of only a few percent of the pore volume below the hydrate-bearing zone are sufficient to create a distinct BSR (e.g. Andreassen et al., 2007; Haacke et al., 2007, and references therein). Higher amounts of gas below a BSR may build up overpressure and lead to low-frequency events in seismic data, since high-frequency components of the seismic energy are absorbed by gas (Geletti and Busetti, 2011). The BSR can be used to derive information about the thermal state at its location, including the local and regional heat flow as well as thermal anomalies that are indicated by a BSR out of equilibrium due to higher or lower temperatures and fluid flow (Hyndman et al., 1992; Grevemeyer and Villinger, 2001; Wood et al., 2002).

The formation of two or more BSRs located a few tens of meters above each other has been reported from multiple sites (Foucher et al., 2002; Popescu et al., 2006; Geletti and Busetti, 2011), but their causes are not well understood. In most of these studies, the shallowest BSR is considered as the seismic manifestation of the current base of the gas hydrate stability zone (BGHSZ). The additional BSRs are usually weaker in amplitude and can occur with normal or reversed polarity compared to the seafloor reflection. Suggested explanations for the occurrence of multiple BSRs include different gas compositions (Geletti and Busetti, 2011), top and base of the free gas zone (Tinivella and Giustiniani, 2013), top and base of the hydrate-bearing zone (Posewang and Mienert, 1999), overpressure conditions below the depth of the theoretical BSR (Tinivella and Giustiniani, 2013), BSRs unrelated to gas and gas hydrates (Berndt et al., 2004), and BSRs representing former stable conditions for the BGHSZ (Foucher et al., 2002; Netzeband et al., 2005; Popescu et al., 2006). The latter are often related to distinct changes in the glacial-interglacial cycles (Bangs et al., 2005; Davies et al., 2012).

One of the most spectacular examples of multiple BSRs has been reported by Popescu et al. (2006) for the Danube deep-sea fan in the Black Sea, where up to four different BSRs with reversed amplitude are observed. These BSRs were observed in small segments of 2D seismic profiles that crossed a buried channel-levee system in water depths between 1000 m and 1500 m. All BSRs observed in that study are sub-parallel to the seafloor. Popescu et al. (2006) excluded that these BSRs reflect gas hydrate layers for different gas compositions as they are in sharp contradiction with the general background of the gas composition in the study area. The authors concluded that the deeper BSRs are paleo-BSRs corresponding to stable cold climatic episodes of the Black Sea. In their model, the authors calculated the depth of the BGHSZ based on the current seafloor for sealevel lowstands and bottom-water temperatures for different glacial periods, but they assumed a constant sedimentary overburden during the glacial cycles.

Here, we show that the deeper BSRs are unrelated to the current seafloor topography and that the sediment overburden was not constant during the last glacial cycles. We use new 2D seismic data to investigate the character and distribution of multiple bottom-simulating reflections in the vicinity of a channel-levee system in the Danube deep-sea fan. The multiple BSRs consequently require a new explanation taking into account the asymmetric deposition of the Danube levee sediments. Therefore, we tested two hypotheses that may explain the formation of the lower BSRs. The first hypothesis is that overpressured gas pockets exist below the BSR leading to different depths at which hydrates are stable. The second hypothesis is that the multiple BSRs are indeed paleo-BSRs caused by the complex interplay between bottom water temperature and sealevel variations and the depositional history of the Danube deep-sea fan during glacial periods.

2. Geological Setting

The deep-sea fans of the Danube and Dniepr rivers are located in the northwestern part of the Black Sea (Fig. 1) and began to develop at about 900 ka BP (Winguth et al., 2000). They are the result of sediment discharge by the rivers Danube, Dniepr, Dniestr and Bug during the last glaciation (Winguth et al., 2000; Popescu et al., 2001). The continental shelf is up to 120 km wide and the Danube deep-sea fan developed downslope of the shelf break at about 100 m water depth down to the abyssal plain in 2200 m water depth (Wong et al., 1997). The canyons and channels of the fan are characterized by erosional processes on the upper slope and by depositional processes on the middle and lower slope (Popescu et al., 2001). Eight seismic sequences were identified in the Danube deep-sea fan, consisting of stacked channel-levee systems, overbank sediments and mass transport deposits (Wong et al., 1997).

The most recent active channel of the Danube fan is the Danube channel (Fig. 1), which was connected to the mouth of the Danube river by the Viteaz canyon at the shelf break (Popescu et al., 2001). The erosive Viteaz canyon terminates in a channel-levee system at about 800 m water depth (Lericolais et al., 2013) and developed during the last glacial period about 25 ka BP when the sealevel was up to 150 m lower than today (Winguth et al., 2000). As observed in other river fans of the northern hemisphere, the right-hand (western) levees are more pronounced than the left-hand (eastern) levees because of the Coriolis force (Popescu et al., 2001). Several older channels can be identified from the bathymetry such as a channel westwards of the Danube channel named SUGAR channel in this study (Fig. 1).

The upper limit of the gas hydrate stability zone (GHSZ), calculated for the observed bottom water temperature of 9 °C and a limnic pore water salinity of 3, is located in a water depth of 665 m. This is supported by the observation of numerous gas flares in water depths shallower than 665 m and much fewer gas flares at greater water depth in parts of the Danube fan (Bialas, 2014), and other areas of the Black Sea such as the Dniepr fan (Naudts et al., 2006) or the Don-Kuban fan (Römer et al., 2012). The expelled gas is primarily composed of methane of biogenic origin with concentrations of 99.1 – 99.9 % (Poort et al., 2005; Römer et al., 2012; Bialas, 2014).

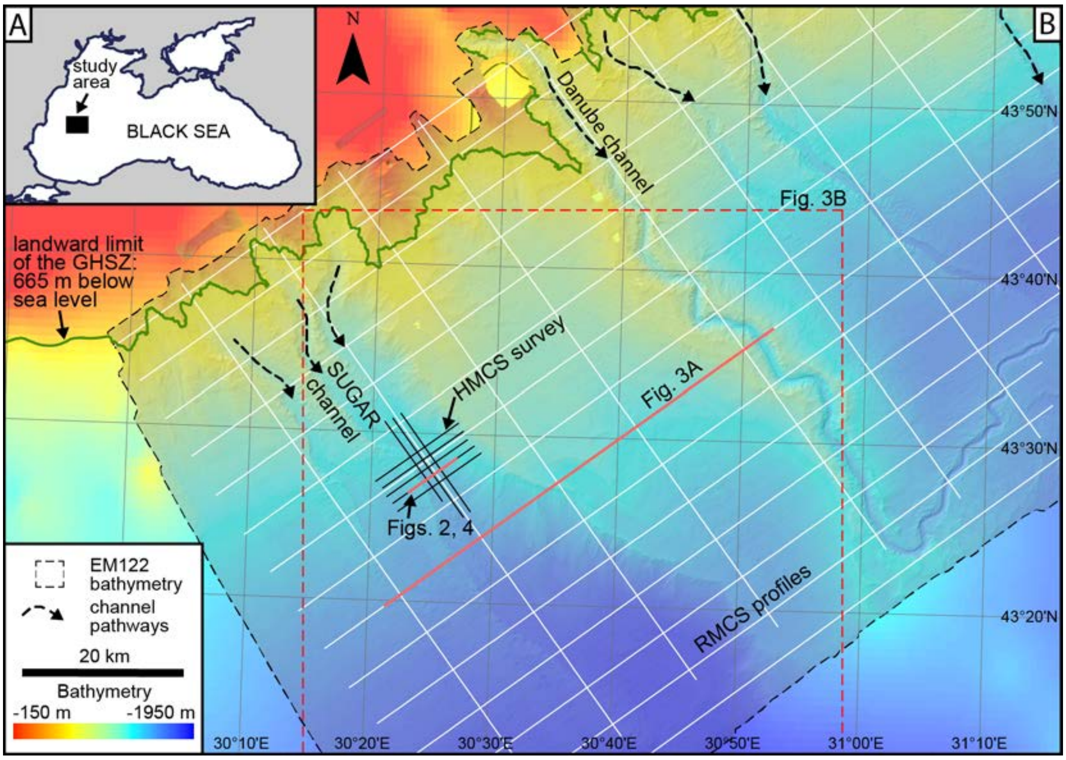

Fig. 1 A: Location of the study area in the northwestern Black Sea. B: Overview map of the study area in the Danube deep-sea fan. GHSZ = gas hydrate stability zone, HMCS = 2D high-resolution multichannel seismic survey, RMCS = 2D regional multichannel seismic survey. Bathymetry and seismic data were acquired during R/V Maria S. Merian cruise MSM34 in 2013-2014.

3. Data and Methods

All data presented in this study were collected during cruise MSM34 onboard the German research vessel MARIA S. MERIAN from December 2013 to January 2014. A total of 26 2D regional multichannel seismic (RMCS) profiles were recorded using a 1050 m long streamer with 168 channels and a group distance of 6.25 m (Bialas, 2014). Sixteen profiles were acquired across the Danube fan with a spacing of 5 km and lengths of 45 – 110 km, and 10 profiles were acquired in downslope direction with a length of 40 – 70 km (Fig. 1).

Additionally, a 2D high-resolution multichannel seismic survey (HMCS) was acquired using a 62.6 m long streamer with 40 channels and a group distance of 1.56 m. Eight profiles were recorded over an area of two merging channel-levee systems: three profiles along the channel's direction (14 km length each) and five profiles across the channels (11 km length each). A 105/105 in^3 GI gun was used as a source for the RMCS survey, and a 45/45 in^3 GI gun was used for the HMCS survey. The shot interval was 5 s. After navigation processing, Omega (WesternGeco) was used for signal-processing, stacking, semblance picking (only RMCS) and true-amplitude time migration. No gain was applied during processing. The RMCS data has a CDP spacing of 3.12 m and a center frequency of 70 Hz, and the HMCS data has a CDP spacing of 1.56 m and a center frequency of 130 Hz. As the short streamers do not allow for semblance analysis of the HMCS data the velocity information of the RMCS profiles was extrapolated to the HMCS area. Both the RMCS and HMCS profiles were converted from time to depth domain using the RMCS-derived velocity information and cross-checked with P-wave velocities from ocean bottom seismometers that were available in the study area (Bialas, 2014).

Multibeam bathymetry data were collected during the entire RMCS survey using the ship-mounted EM122 echosounder (Kongsberg). The resulting map comprises a grid of 25 m x 25 m resolution.

In order to calculate an average temperature gradient, we assumed that the location of the shallowest BSR corresponds to the present BGHSZ. We fitted the methane hydrate phase boundary that was calculated using the SUGAR Toolbox (Kossel et al., 2013) for different temperature gradients in the interval between the seafloor and the shallowest BSR.

4. Results

The multiple BSRs were imaged by three different recording systems, which confirm their existence more than 10 years after their discovery as described by Popescu et al. (2006). This observation also rules out that the BSRs are ephemeral features, or the product of incorrect processing or artifacts.

4.1 Character and distribution of multiple BSRs

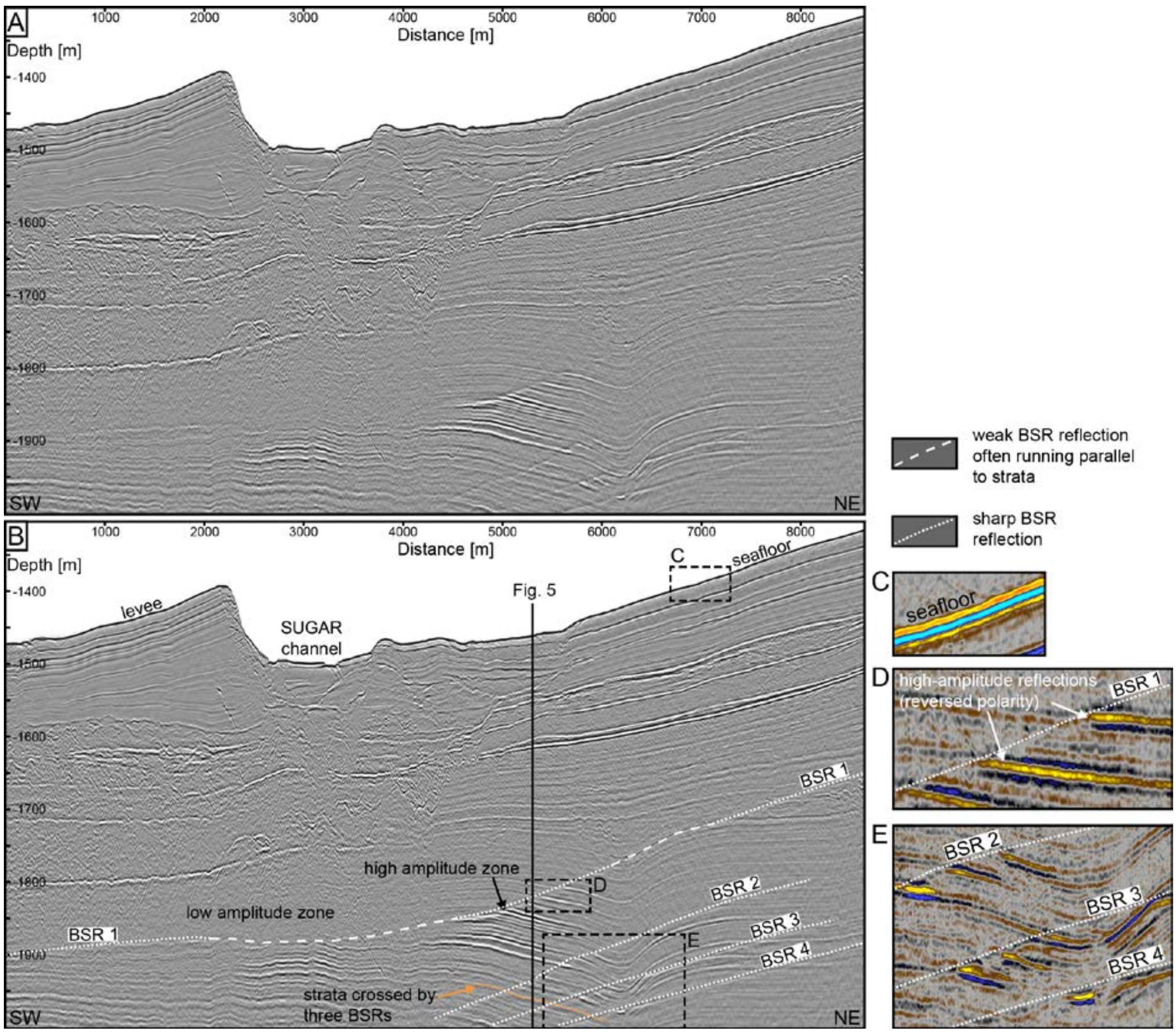

Fig 2 A: 2D HMCS line 1107 across the SUGAR channel-levee system. The location is shown in Fig. 1. B: Interpreted section showing the general character of the four stacked multiple BSRs. C-E: Insets with different colour scale highlight the positive polarity of the seafloor (C) and the negative polarities of the reflections underneath the shallowest BSR 1 (D) and BSRs 2-4 (E).

The shallowest BSR occurs in depths of about 320-380 m below the seafloor and generally runs parallel to the seafloor. It can be identified in large patches throughout the Danube deep-sea fan, as already observed in previous studies (Popescu et al., 2006; Bialas, 2014). The reflection amplitudes are generally low in an almost transparent seismic facies above the BSR, while they are high and of reversed polarity below the BSR (Figs. 2C, D). The appearance of the BSR is continuous and sharp where it crosscuts strata (Fig. 2B). Where it is parallel to the strata, the BSR is characterized by an abrupt amplitude increase with depth. The strongest amplitudes below the BSR are observed underneath the eastern levee, where several high-amplitude reflections pass from below the BSR into the transparent zone while undergoing a phase reversal at the BSR (Fig. 2D). The observed increased amplitudes below the BSR are often limited to individual reflectors that underlie a reflector of weaker amplitude (Fig. 2D).

Three additional BSRs are observed in the MCS data, named BSR 2-4 from top to bottom, and underlying the shallowest BSR described above (Figs. 2B, E). These BSRs are generally weaker in amplitude compared to the shallowest BSR, but they also represent a sharp and continuous boundary towards increased amplitudes below. Each of the additional BSRs shows reversed polarity compared to the seafloor. Some BSRs cross the same strata (Fig. 2B) while they exhibit slightly varying individual dips.

The stack of BSRs 2-4 is only observed in the well-stratified levee deposits of a buried channel-levee system (BCL) identified in the subsurface (Fig. 3). The BSRs are generally limited to the western levee of the BCL, but on few RMCS profiles we also observed the BSR stack in the eastern levee (Fig. 3B) where the overburden is thicker compared to the western levee (Fig. 3A). The multiple BSRs are not observed in or underneath the channel axis, and the reflections of all BSRs fade out where they intersect with the base of the BCL (Fig. 3A).

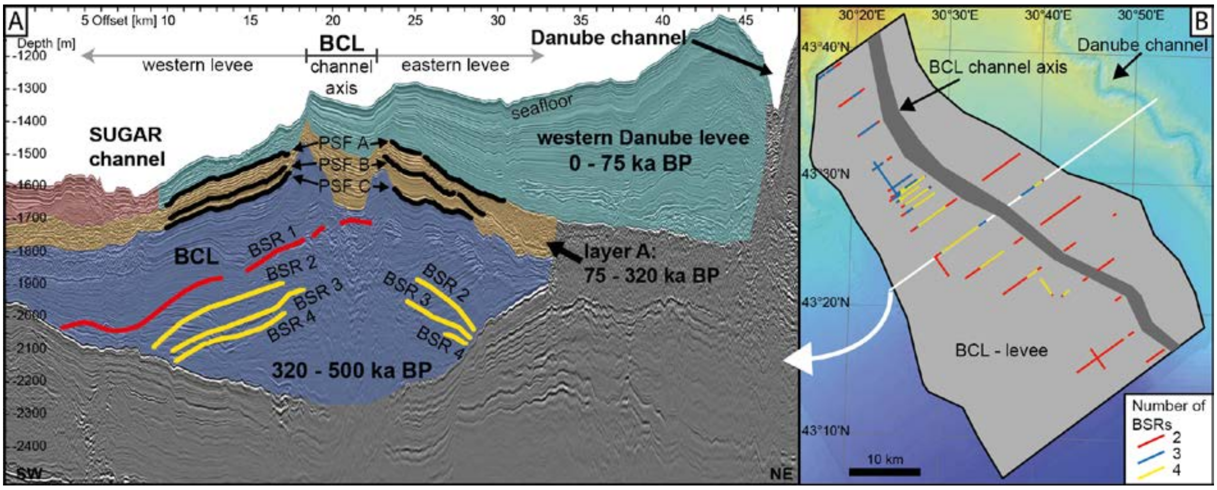

Fig. 3 A: 2D RMCS line 09 across the SUGAR channel (red unit) and the western Danube channel levee (green unit) in the northeast. A buried channel-levee system (BCL) is identified in the subsurface (blue unit), underneath layer A (brown unit). The multiple BSRs (yellow lines) are solely observed in the levees of the BCL. Time frames for the deposition of the different facies units are adapted from the interpretation of Winguth et al. (2000) (Figure 4 in

their study). Three paleo seafloors were defined for the modelling of the BGHSZ under paleo conditions (black lines PSF A-C). B: Extent of the BCL based on seismic data and highlighting the occurrence of more than one BSR. Locations of A and B are shown in Fig. 1. An uninterpreted version of the seismic section is presented in the Supplementary material.

The BCL is overlain by the outer levee deposits of the Danube channel (Fig. 3A). A sediment unit (layer A) exists between the BCL and the Danube levee and is characterized by an average thickness of about 80 m. The structure of layer A is homogeneous and layered sub-horizontally. Earlier studies by Winguth et al. (2000) indicate the depositional ages of the main depositional units in this area. The Danube levee was deposited over the past 75 ka during the last major glacial cycle, and the BCL was deposited during the period of 500 – 320 ka BP. Layer A consequently was deposited during the period of 320 – 75 ka BP.

4.2 Thermal modelling

The thermodynamic stability of gas hydrates depends on local pressure, temperature, gas composition, and pore water salinity (Sloan, 1998). In the Black Sea the bottom-water temperature of 9 °C is well constrained by numerous studies and is remarkably uniform on regional and temporal scales (Degens and Ross, 1974; Vassilev and Dimitrov 2002). The gas composition in our model is assumed to be pure methane because of the $\delta^{13}C$ values of CH_4 between -84‰ and -70‰ observed in the surface sediments at seeps and in the BSR areas of the study area (unpublished data). Due to past limnic phases of the Black Sea, the pore water salinity in the sediments decreases rapidly from ~22.3 at the seafloor (Özsoy and Ünülata, 1997) to ~2-5 in shallow subbottom depth as observed in DSDP cores (Calvert and Batchelor, 1978) and surface sediment cores from our study area (Soulet et al., 2010). A geothermal gradient of 24.5 °C/km ± 0.5 °C/km fits best along the northeastern area of the SUGAR channel at HMCS line 1107 where the slope is gentle and the topographic effects are minimal (Fig. 4A). Below the SUGAR channel and its western levee, we observe an increasing mismatch with the BSR-derived temperature of up to 2 °C lower compared to the regional temperature field (Fig. 4A).

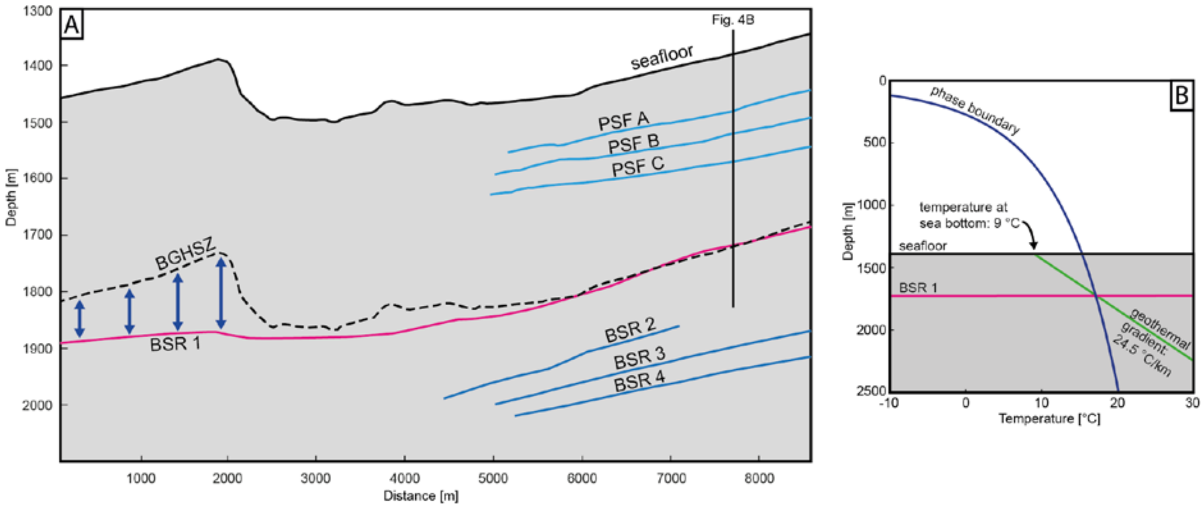

Fig. 4A Interpretated 2D HMCS line 1107 from Fig. 2, reduced to the relevant horizons of this study. The BSR is plotted as a pink line. The theoretical BGHSZ fits best to the BSR with a regional geothermal gradient of ~24.5 °C/km below the northeastern levee where the topographic effect is expected to be minor. Towards the channel and western levee, the mismatch between the shallower base of the gas hydrate stability zone (BGHSZ) and the bottom simulating reflector (BSR) indicate a local thermal gradient that is up to 5 °C/km lower compared to the regional temperature field (blue arrows). B: Phase diagram illustrating the stability conditions of methane hydrates at the location depicted in A. PSF = paleo seafloor.

5. Discussion

5.1 Thermal state of the channel-levee system

With each BSR showing reversed polarities compared to the seafloor reflection and increased amplitudes underneath, we can confirm that the impedance contrast causing the crosscutting BSRs in the seismic data is most likely caused by free gas. The regional temperature gradient of ~24.5 °C/km that we derived from the BSR temperature at the location of the multiple BSRs is lower compared to temperature gradients of other studies (30 °C/km; Popescu et al., 2006; Vassilev and Dimitrov, 2002). A possible explanation for this difference might be incorrect velocity estimates used by Popescu et al. (2006) for depth conversion of their seismic data. Lacking alternative velocity information, Popescu et al. (2006) converted travel time to depth by assuming velocities between 1600 m/s and 1800 m/s based on velocity profiles from the Storegga site offshore Norway published in Posewang and Mienert (1999), and from the Dniepr deep-sea fan as published in Lüdmann et al. (2000). However, our velocity analysis of the RMCS profiles and OBS data indicate that the seismic velocity increases from 1485 m/s at the seafloor up to 1950 m/s at BSR level in 380 m depth. Thus, the depth of the BSRs might be underestimated in the studies of Popescu et al. (2006), which consequently leads to a higher geothermal gradient derived from the shallower BSR.

Below the western levee of the SUGAR channel, the BSR-derived temperature indicates a local geothermal gradient even lower than ~24.5 °C/km (Fig. 4A). This observation suggests that the gas hydrate system of the Danube deep-sea fan is not in a steady state. The misfit may have been caused by rapid levee deposition. However, in the multiple BSR area, the temperature field is likely equilibrated, as the BSR 1 is in good agreement with the theoretical BGHSZ. This match between predicted and observed BSR 1 is particularly important. In the absence of deep sources for heat flow variations (e.g. volcanic intrusions), it is expected that with increasing depth the thermal field is increasingly in steady state, as the effects of surface processes are averaged out by thermal diffusion.

The levee deposits of the Danube fan extend far into the area of the SUGAR channel. With increasing distance from the Danube channel, the thickness of the levee deposits decreases, which leads to a thicker overburden above the eastern levee of the BCL compared the western levee (Fig. 3). Considering the thickness variations of individual sedimentary layers (Figs. 2 and 3), it is evident that the sediment load above the multiple BSRs grew during the past glacial cycles and was not constant as stated by Popescu et al. (2006). As we also observe multiple BSRs in the eastern levee of the BCL modeling these BSRs from current seafloor depth would require high variations of pressure and temperature. This introduces large errors when the BSRs are linked to ranges of lower bottom-water temperatures during stable cold climate periods, as noted by Popescu et al. (2006).

5.2 Multiple BSRs due to overpressure compartments

Methane hydrates are stable under high pressure and low temperature (Kvenvolden, 1995), with temperature controlled by bottom-water temperature and the regional geothermal gradient. Pressure, on the other hand, is mainly controlled by hydrostatic pressure in the relevant sediment depths (Berndt, 2005) and hence, increases linearly with depth. As a result, the base of gas hydrate stability is defined by a sharp boundary. If, however, the pore pressure is above hydrostatic conditions, the base of gas hydrate stability moves towards greater depths. Fluid overpressure can be caused by fluid volume changes (i.e. due to temperature increase, fluid hydrocarbon generation from kerogen, or H_2O release in the smectite-illite transformation reaction), fluid movements (due to buoyancy or osmosis), or compaction (e.g. reservoir compaction due to tectonic stress or rapid deposition) (Tacket and Puckette (2012) and references therein). Overpressures can also be caused by free gas, for which the amount of pressure increase depends on the height of the gas column. The presence of free gas is not only indicated by the BSRs but also by bright spots of varying intensity, which are observed beneath each BSR (e.g. the high amplitude zone in Fig. 2).

Stepped or tiered overpressure systems have been reported from several sedimentary basins, such as the North Sea Basin (3.4 km depth; Heritier et al., 1979), the Sacramento Basin (1.8 km depth; Tacket and Puckette, 2012), or the Anadarko Basin (3 km depth; Al-Shaieb et al., 1994). These overpressure systems are linked to permeability barriers in the sediment column and are observed in much greater depths compared to the typical thickness of the GHSZ, which ranges between 0 m and 900 m (e.g. Wallmann et al., 2012).

In order to test whether overpressured compartments in the subsurface may form pockets of stable gas hydrates, we calculated a 1D model for a location in 1460 m water depth with four sharp BSRs (location in Fig. 2B) and a regional geothermal gradient that is assumed to be stable at 24.5 °C/km. The gas composition for all BSRs was assumed to be pure methane and the pore water salinity was set to 5.

The resulting phase boundary for stable methane hydrates at this location is in a depth of 1827.5 m below sea surface, fitting well with the shallowest BSR in a depth of 1828 m (Fig. 5). The required pressures for stable methane hydrates at BSRs 2-4 are the sum of the hydrostatic pressure at the respective depths and the overpressures $P_{DBSR2,3,4}$.
Based on the overpressures required for stable methane hydrates above the deeper BSRs, we calculated the required height of the gas column generating this pore overpressure:

$$H_{BSR2,3,4} = P_{DBSR2,3,4}/g * (\rho_w - \rho_{CH_4}) \qquad (1)$$

where $H_{BSR2,3,4}$ is the height of the gas column, $P_{DBSR2,3,4}$ are the overpressures for each of the multiple BSRs, g is the gravitational acceleration (9.81 m/s^2), ρ_w is the density of the formation water (1025 kg/m^3), and ρ_{CH_4} is the density of methane, which depends on the temperature and pressure. ρ_{CH_4} was thus calculated separately for P and T at each BSR level, using the SUGAR toolbox (Kossel et al., 2013).

Table 1 Overpressure parameters required for stable methane hydrates at each BSR level.

Reflector	Depth below sea surface [m]	Hydrostatic pressure [MPa]	Total required pressure [MPa]	P_D [MPa]	Lithostatic pressure[a] [MPa]	Density of methane [kg/m³]	Gas column height [m]
Seafloor	1460 +/- 5						
BSR 1	1828 +/- 10						
BSR 2	1941 +/- 10	19.5	25.7	6.2	22.6 – 23.6	~196.9	~766
BSR 3	1980 +/- 10	19.9	28.9	9.0	23.9 – 25.0	~211.7	~1134
BSR 4	2011 +/- 10	20.2	31.8	11.6	24.5 – 25.6	~223.1	~1474

[a]lithostatic pressure derived from density using a density-velocity correlation (details are provided in the Supplementary materials)

The 1D calculation for the selected site shows that the calculated gas column heights for piercing the phase boundary for stable methane hydrates are 24-36 times higher than the vertical distance between two BSRs. For example, the vertical distance between BSRs 2 and 3 is ~39 m, whereas the required height of the gas column underneath BSR 2 would be ~766 m (Table 1). This gas column height exceeds the range of gas column height required for fault reactivation at Blake Ridge (150-290 m; Hornbach et al., 2004), seal failure in the North Sea (263 m; Karstens and Berndt, 2015), or sediment doming offshore New Zealand (37-121 m; Koch et al., 2015).

Data for lithostatic pressure in the Danube fan were unavailable for this study. Therefore, we calculated likely lithostatic pressure profiles from density using a density-velocity correlation (table 1). More details of the calculation are provided in the Supplementary materials. Furthermore, we compared the lithostatic pressures to measurements from the Mississippi delta in the Gulf of Mexico, which is located in a comparable setting to the Danube deep-sea fan. During IODP expedition 308, measured lithostatic pressures were in the order of 18.6 kPa/m (Behrmann et al., 2006). The lithostatic pressures (Fig. 5) show that the required pressures for stable gas hydrates at the multiple BSRs likely exceed lithostatic pressure.

DSDP cores from site 379A show an increase in salinity into the hypersaline stage starting at ~350 m below the seafloor (Calvert and Batchelor, 1978), which is in the depth range of the deeper BSRs at our study site. An increase in pore water salinity results in a shift of the phase boundary towards higher pressures (Fig. 5). The top of the hypersaline stage lies probably in greater depth at the Danube fan compared to the DSDP site, due to greater sediment thickness.

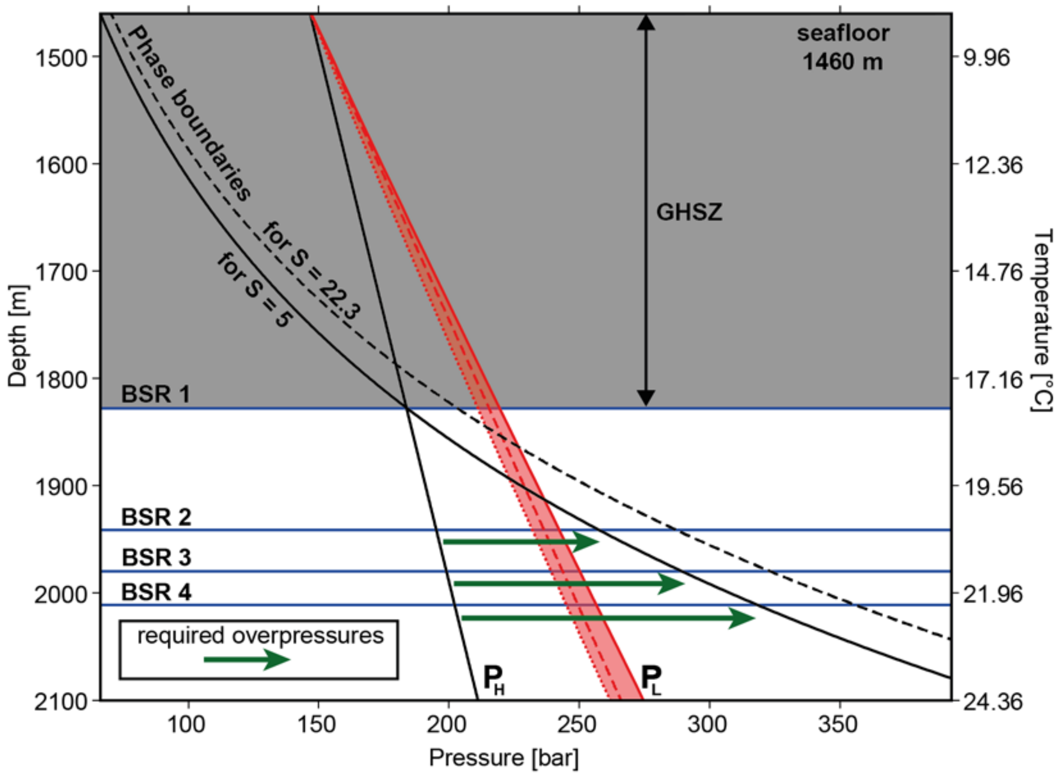

Fig. 5 Phase diagram for pure methane hydrates at our model site in 1460 m water depth. The calculated BGHSZ of our 1D model fits well with the location of BSR 1. The required overpressures at each BSR level (green arrows, see Table 1) are likely above lithostatic pressure for the multiple BSRs (P_L, red area, calculated with a density-velocity correlation based on two different approaches as described in the Supplementary material. Red dashed line: lithostatic pressure measured in the Gulf of Mexico). The increased pore water salinity (S) is plotted as a dashed black line, indicating a further increase in overpressure with increasing salinity for stable methane hydrates at the BSR levels. The location for this model is shown in Fig. 2B.

Based on our calculations, it is unlikely that pockets with overpressured gas are present in the Danube fan area and cause the observed BSRs. Lithological boundaries, which would support the formation of pressure compartments, are not observed. Instead, the same strata are crossed by two or more BSRs at the same location (Fig. 2). Some patches below each BSR may be gas-charged as suggested by their high amplitude contrast and polarity change. However, the height of the gas column beneath each BSR appears to be small, as indicated by the overall small amplitude attenuation below each BSR with almost no loss in frequency content.

5.3 Multiple BSRs caused by temporally changing pressure and temperature conditions in different limnic phases

If the multiple BSRs can be linked to events of climate change (i.e., sealevel variations, changes in bottom water temperatures), the sedimentation above the BCL has to be taken into account. The deposition of the western Danube levee above the BCL lead to an asymmetrical growth of the overburden above the BCL, which is thicker towards the Danube channel in the northeast (Fig. 3). Deposition of the western levee occurred over a relatively short time of 75 ka BP during the last major sealevel lowstand (e.g. Winguth et al., 2000; Popescu et al., 2001). Therefore, we need to find the corresponding paleo seafloors (PSFs) for these events. These horizons can be found in layer A, which is located between the BCL and the base of the Danube levee (Fig. 3). This layer was well mapped by cross-correlating the available seismic data along the study area. The thickness of this layer is in the range of ~70 m to ~120 m. According to Winguth et al. (2000), the age of this layer is in the range of 75 ka to 320 ka and thus spans at least three major limnic phases of the Black Sea (Manheim and Shug, 1978; Muratov et al., 1978).

Due to the large uncertainty of the real age of layer A (drilling data are not available), we defined and picked three reasonably spaced horizons representing the PSFs in layer A. We used these PSFs for modelling the BGHSZ at paleo levels: The upper boundary of layer A was assumed to correspond to the paleo seafloor for BSR 2 (PSF A), the lower boundary was assumed to correspond to BSR 4 (PSF C), and a horizon in the center of layer A (PSF B) was assumed to correspond to BSR 3 (Fig. 3).

We observed that in the multiple BSR area, the present-day BSR is stable and follows the temperature field (Fig. 4A). Therefore, it is reasonable to test paleo pressure and temperature conditions for the PSFs as boundary parameters for the paleo BSRs. In our 2D model approach, we calculated the BGHSZ for each of the PSFs under assumed paleo conditions, which included a 120-150 m lower sealevel compared to today (e.g. Ryan et al., 1997; Lericolais et al., 2009) and a lower bottom water temperature than today's 9°C. Poort et al. (2005) inferred a temperature decrease of 2.0-5.5 °C at about 7.1 ka BP, while Soulet et al. (2010) reconstructed 4 °C for the last glacial maximum based on $\delta^{18}O$ porewater data. Because 4 °C is also the density maximum for fresh water, we used this value as a start for the model, but also ran it with higher temperatures of 5 °C and 6 °C. The pore water salinity was kept at 5.

In this approach, the temperature gradient in the sediments was set as a variable, because we expected a higher temperature gradient in the upper sediment column due to the lower bottom-water temperature. By varying the temperature gradients, we fitted the modelled BGHSZ for the individual PSFs to the paleo-BSRs. The model shows a good fit of the BGHSZ models to the corresponding paleo-BSRs for temperature gradients in the range of 35 – 37.5 °C/km at 4 °C bottom water temperature and for a 150 m lower sealevel. The results are shown for the two profiles HMCS line 1107 (Fig. 6 A-C) and RMCS line 09 (Fig. 6 D-F). Lowering the sealevel by only 120 m instead of 150 m results in slightly higher (by ~0.5 °C/km) temperature gradients, whereas an increase of the bottom water temperature by 1 °C results in a reduction of the required temperature gradients by 2.0-2.5 °C/km.

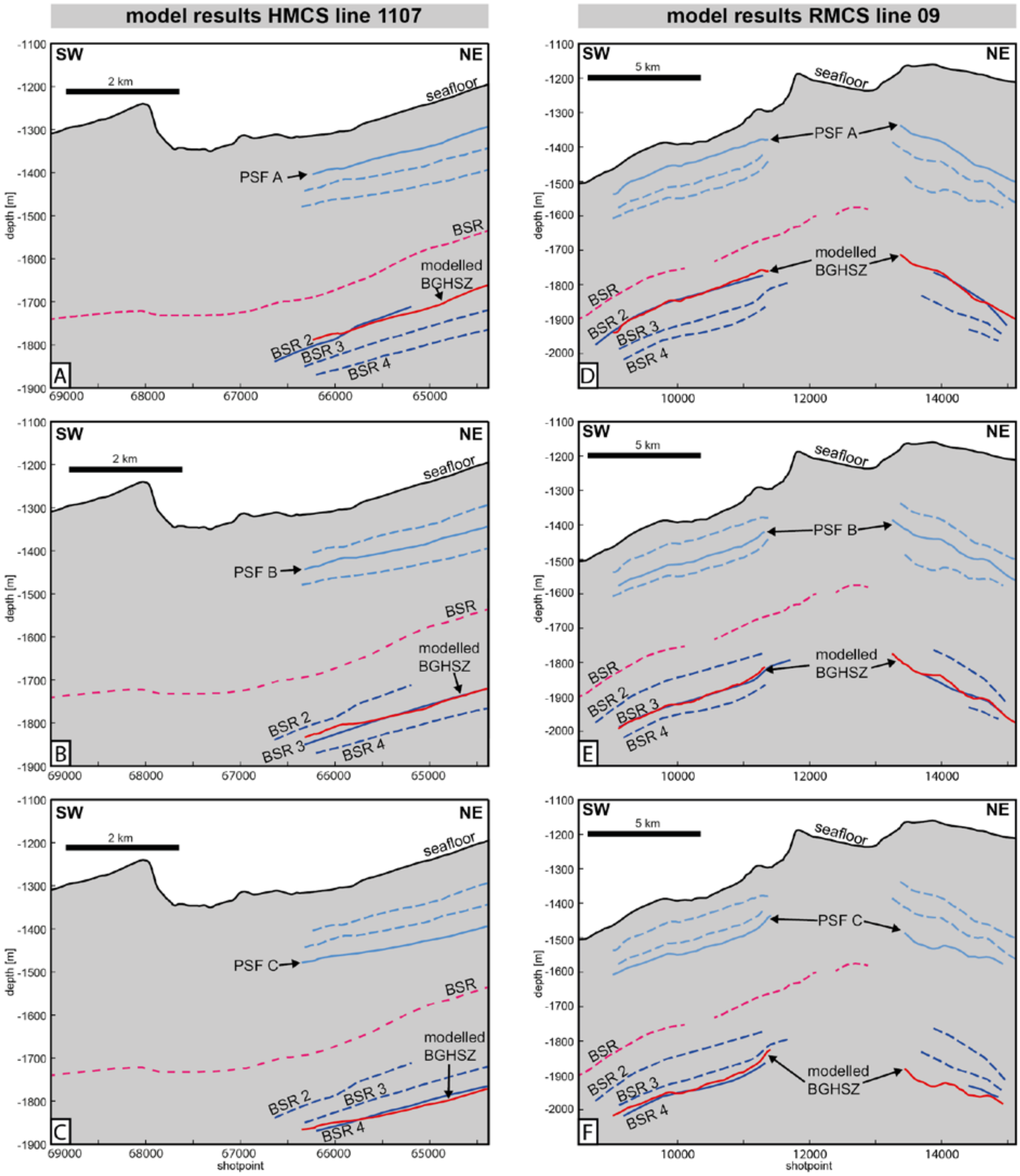

Fig. 6 Model results for matching the paleo BSRs with the paleo seafloors. A-C: Results for HMCS line 1107 near the SUGAR channel. The BGHSZ (red line) is calculated from the paleo seafloor (PSF, light blue) and compared to the paleo BSRs (dark blue). Model parameters are described in the discussion. D-E: Results for RMCS line 09, where the paleo BSR stack is also observed further to the northeast.

Our results show that it is possible to link the paleo BSRs to paleo seafloor horizons in layer A (Fig. 6). The depositional history of layer A indicates that the paleo BSRs reflect stages of stable sealevel lowstands under glacial conditions. The glacial-interglacial cycles are more distinctive in the Black Sea compared to other areas due to the isolation from the

Mediterranean during sealevel lowstands. The preservation of paleo BSRs may have been favored by the development of the Danube deep-sea fan under lacustrine conditions (Popescu et al., 2001) controlled by rapid sealevel changes in the order of 120–150 m.

However, high uncertainties beyond small-scale misfits of modelled BGHSZ and paleo BSRs are associated with our model approach. The largest uncertainties originate from the choice of the PSF horizons, which are exchangeable as they are all deposited sub-parallel. Only drilling into this layer can provide more certainty. The errors of the PSFs and the BSRs are mainly related to uncertainties in the velocities, but also to the picking accuracy, static errors, and imaging problems. High uncertainties of the model are also related to the paleo parameters (bottom-water temperature and paleo sealevel). Taking all these uncertainties into account, we estimate that an average geothermal gradient of 35±5 °C/km best reflects stable conditions for the paleo BSRs.

The question remains whether the derived temperature gradient for the paleo BSRs is reasonable. Even though we have to estimate larger errors for the range of the geothermal gradients, the geothermal gradients are nevertheless higher (35±5° C/km) compared to the regional geothermal gradient derived from the shallowest BSR (24.5 °C/km). The only temperature data that is available from greater depth is from DSDP core 379A in the central Black Sea and is in the range of 32 – 38 °C/km (Erickson and Von Herzen, 1978). These results indicate that the paleo BSRs probably reflect the true geotherm of the Black Sea basin. Today's lower geothermal gradient derived from the shallow BSR temperature is still influenced by the increase of the bottom water temperature from about 4 °C to today's 9 °C since the last glacial maximum (Appendix A, Fig. A1). We therefore suggest that the thermal system in the Danube fan still adapts to this change and is not in steady state .The BGHSZ will probably become shallower over the next tens of thousands of years (also pointed out by Poort et al., 2005) as the geotherm increases due to thermal diffusion.

5.4 Preservation of paleo BSRs

The observation of multiple BSRs, which mimic several older seafloors and are partly at steep angles to the present-day seafloor, provides unequivocal evidence that the BSRs must be old structures. The limited age control that exists for the Danube fan suggests that the BSRs must be at least several 10,000 years old and possibly as much as 300,000 years old. After a change of stability conditions by sediment loading due to rapid deposition, the regional geothermal gradient would start to equilibrate by heat conduction from below the GHSZ. This would lead to the dissociation of the lowermost gas hydrates and latent heat absorbed during the dissociation might subsequently cause cooling from this endothermic reaction. Depending on how high the hydrate saturation above the BSR is, cooling would increasingly buffer the temperature field, but, even with high hydrate saturation the dissipation of the cooling presumably should not take longer than a few decades. Consequently, we conclude that despite buffering by latent heat, it is unlikely that gas hydrates still exist above the paleo BSRs, as they would start to dissociate immediately once they leave the stability field.

Dissociation of hydrates should lead to free gas formation within the former GHSZ, but we do not observe any high amplitude reflections directly above the paleo BSRs. In fact, the paleo BSRs in the high-resolution seismic data are remarkably sharp. This strongly suggests that the amount of gas that was formed by gas hydrate dissociation is very small. It also suggests that the free gas that still exists in the zone below the previous GHSZs has not yet begun to migrate upwards causing todays paleo BSRs. It seems likely that the upward migration of the free gas due to its own buoyancy forces is inhibited by low free gas saturation and a general low permeability of the host sediment. The upward migration of gas is controlled by the irreducible gas saturation S_{GC}, which is typically in the range of 0.01–0.1 (Garg et al., 2008), and has to be exceeded in the pore space to enable gas migration (Wallmann et al., 2012). The largest drop in P-wave velocities occurs at gas concentrations lower than 4% (Andreassen et al., 2007). Therefore the free gas concentrations at each paleo-BSR must be low enough for the free gas not to migrate further upwards, but high enough to cause a clear impedance contrast in seismic data. It is likely that only diffusive transport of dissolved gas plays a role in this setting and that the biogenic gas, which is observed in the organic-rich sediment column, is solely produced within the GHSZ. This is supported by the low vertical permeability of the levee sediments in which the BSRs are located, and by the absence of vertical migration pathways in the seismic data. Gas that is produced underneath the BCL may migrate upslope along coarse-grained sediment deposits such as those encountered in the numerous channels and bases of the channel-levee systems, all of which areas where multiple BSRs are not observed.

6. Conclusions

The existence of previously identified multiple BSRs of the Danube deep-sea fan has been confirmed by new 2D multichannel seismic data. A stack of four BSRs was observed in the levee deposits of a buried channel-levee system. The multiple BSRs do not represent gas composition changes or overpressured compartments, but reflect past pressure and temperature conditions. Our modeling results suggest that temperature effects of rapid sediment deposition rather than bottom-water temperature change or sealevel variations dominate the pressure and temperature conditions leading to the multiple BSRs. These changes are more distinctive in the Black Sea and especially in the Danube area because of the isolation of the Black Sea from the Mediterranean during sealevel lowstands. Because hydrate dissociation may not occur for several thousands of years, such paleo BSRs remain well defined in seismic data. We propose that small amounts of free gas are present beneath each of the paleo BSRs. The gas saturation is high enough to cause an impedance contrast in seismic data, but low enough to inhibit buoyancy-driven upward migration. The paleo BSRs possibly reflect the real geotherm in the order of 35±5 °C/km, which is higher than the local geotherm of 24.5±0.5 °C/km derived from the shallowest (current) BSR. This also suggests that the Danube area is not in thermal steady state and still adapting to increasing bottom water temperatures since the last glacial maximum.

Acknowledgements

The research leading to these results has received funding from the European Union Seventh Framework Programme (FP7/2007-2013) under the MIDAS project, grant agreement no. 603418, from the German Ministry of Education and Research (BMBF) and from the Federal Ministry of Economy and Energy (BMWi) through the SUGAR project (grant nos. 03G0819A, 03SX320A, 03G0856A). The RMCS line 09 was kindly provided by the Institute of Marine Science and Technology (IMST-Seislab) of the Dokuz-Eylül University, Izmir, Turkey. We would like to thank the captains and crew of RV MARIA S. MERIAN cruise MSM34 as well as the GEOMAR lab technicians for their excellent support. We thank reviewers Marc de Batist and Ingo Pecher and editor Peter Shearer for their constructive comments that greatly helped to improve the manuscript.

Appendix A

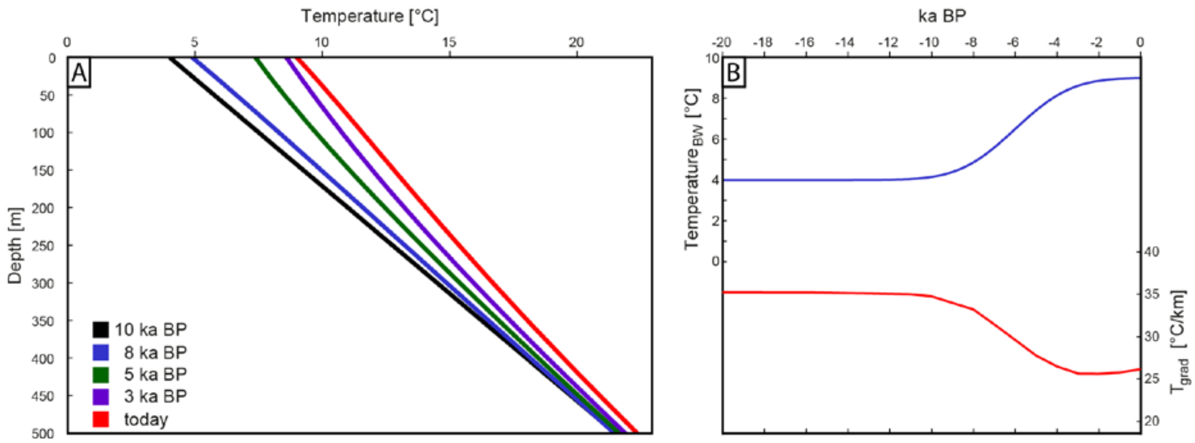

Fig. A1 A: Bottom water warming from 4 °C to 9 °C and the change of the sediment temperature with depth since the last glacial maximum plotted for five timesteps. B: Bottom water warming (blue curve) and the temperature gradient of the top 400 m of sediments (red curve).

Model description

The heat flow in the sediment was simulated using the 1-D non-steady state transport equation:

$$\frac{\partial T}{\partial t} = \frac{\partial}{\partial x}\left(\frac{\lambda}{c_P}\frac{\partial T}{\partial x} + uT\right) \tag{1}$$

where t is time, x is the depth, T is the temperature, λ is the thermal conductivity of the sediment matrix, u is the advection velocity, and c_p is the thermal capacity of the sediment matrix. In Equation 1, the first term on the right side is equivalent to Fourier's law of conductive heat transport and the second term represents the convective heat transport due to advection (i.e. burial of bulk sediment).

The thermal conductivity λ and the heat capacity c_p of the bulk sediment were calculated from the respective values for solid phase and porewater, weighted by the respective volume fractions in the sediment:

$$\lambda = \phi\lambda_f + (1-\phi)\lambda_s \tag{2}$$

where λ_f is the thermal conductivity of seawater and λ_s is the thermal conductivity of the solid phase, and

$$c_p = \phi c_f + (1-\phi)c_s \tag{3}$$

where c_f is the heat capacity of seawater and c_s is the heat capacity of the solid phase.

Sediment porosity was calculated in the model using an empirical relationship (Boudreau, 1997):

$$\phi(z) = \phi_L + (\phi_0 - \phi_L)e^{-\beta z} \tag{4}$$

where ϕ_0 is the porosity at the sediment surface (x=0), ϕ_L is the porosity at a sediment depth of x=L, and β is the porosity attenuation coefficient (see Table A1 for the parameter values).

The partial differential equation was solved using the 'pdepe' function of Matlab®. A constant bottom water temperature (T_{BW}) was chosen as upper boundary condition and a constant conductive heat flow (F_L) at the lower boundary.

Table A1: Summary of the parameter values used in the heat flow model

Parameter	Symbol	Value [Unit]	Reference
Length of the model column	L	15,000 [m]	-
Water depth	p	1500 [m]	This study
Salinity of bottom water	S_{BW}	22.3	Degens & Ross (1974)
Salinity in the GHSZ	S_{GHSZ}	3	[a]
Porosity at sediment surface (x=0)	ϕ_0	0.7	based on DSDP42b Site379
Porosity at base of sediment (x=L)	ϕ_L	0.38	based on DSDP42b Site379
Porosity attenuation coefficient	β	0.00008 [1/cm]	based on DSDP42b Site379
Heat capacity of seawater	c_f	$4.14 \cdot 10^6$ [J/(m^3 K)]	Kossel et al. (2013) [b]
Heat capacity of sediment	c_s	$2.15 \cdot 10^6$ [J/(m^3 K)]	Kossel et al. (2013)
Thermal conductivity of seawater	λ_f	0.63 [W/m/K]	Kossel et al. (2013) [b]
Thermal conductivity of sediment	λ_s	1.65 [W/m/K]	Kossel et al. (2013) [c]
Sedimentation rate	u	0.03 [cm/a]	Soulet et al. (2010) [d]
Temperature of bottom water (x=0)	T_{BW}	9 [°C]	Degens & Ross (1974)
Heat flow at base of sediment (x=L)	F_L	44 [mW/m^2]	Sclater et al. (1980)

[a] Salinities of 2-5 are reported for the Danube area and DSDP42b Site 379. A value of 3 was used in the calculations. Variations between 2 and 5 do not alter the results significantly.

[b] Average value for p, T, S range in the GHSZ.

[c] 1.3 W/m/K for Black Sea sediments with a porosity of 0.3.

[d] Average value for the past 10-15 ka.

References

1. Al-Shaieb, Z., Puckette, J.O., Abdalla, A.A., and Ely, P.B., 1994. Megacompartment Complex in the Anadarko basin: a completely sealed overpressured phenomenon. In: Ortoleva, P.J. (Ed.), Basin compartments and seals. AAPG Memoir 61, 55-68.

2. Andreassen, K., Nilssen, E. G., and Ødegaard, C. M., 2007. Analysis of shallow gas and fluid migration within the Plio-Pleistocene sedimentary succession of the SW Barents Sea continental margin using 3D seismic data. Geo-Marine Letters 27, 155–171, doi: 10.1007/s00367-007-0071-5

3. Bangs, N.L.B., Musgrave, R.J., and Tréhu, A.M., 2005. Upward shifts in the southern Hydrate Ridge gas hydrate stability zone following postglacial warming, offshore Oregon. Journal of Geophysical Research 110, 13p, doi: 10.1029/2004JB003293

4. Behrmann, J., Flemings, P.B., and John, C.M., 2006. Rapid sedimentation, overpressure, and focused fluid flow, Gulf of Mexico Continental Margin. Scientific Drilling 3, 12-17, doi: 10.2204/iodp.sd.3.03.2006
5. Berndt, C., Bünz, S., Clayton, T., Mienert, J., and Saunders, M., 2004. Seismic character of bottom simulating reflectors: examples from the mid-Norwegian margin. Marine and Petroleum Geology 21, 723-733, doi: 10.1016/j.marpetgeo.2004.02.003
6. Berndt, C., 2005. Focused fluid flow in passive continental margins. Philosophical Transactions of the Royal Society A 363, 2855-2871, doi: 10.1098/rsta.2005.1666
7. Bialas, J. (ed.), 2014. FS MARIA S. MERIAN Fahrtbericht / Cruise Report MSM-34 / 1 & 2 SUGAR Site. Berichte aus dem GEOMAR Helmholtz-Zentrum für Ozeanforschung Kiel Nr. 15.
8. Calvert, S. E., and Batchelor, C. H., 1978. Major and minor element geochemistry of sediments from Hole 379A, Leg 42B, Deep-Sea Drilling Project. Initial Reports of the Deep Sea Drilling Project 42 Part 2, 527 – 541.
9. Degens, E.T., and Ross, D.A., 1974. The Black Sea – Geology, Chemistry, and Biology. The American Association of Petroleum Geologists, Tulsa, USA.
10. Davies, R.J., Thatcher, K.E., Armstrong, H., Yang, J., and Hunter, S., 2012. Tracking the relict bases of marine methane hydrates using their intersections with stratigraphic reflections. Geology 40, 11, 1011-1014, doi: 10.1130/G33297.1
11. Erickson, A.J., and Von Herzen, R.P., 1978. Downhole temperature measurements and heat flow data in the Black Sea; DSDP Leg 42B. Initial Reports of the Deep Sea Drilling Project 42 Part 2, 1085-1103.
12. Foucher, J.P., Nouzé, H., and Henry, P., 2002. Observation and tentative interpretation of a double BSR on the Nankai slope. Marine Geology 187, 161-175, doi: 10.1016/S0025-3227(02)00264-5

13. Garg, S. K., Pritchett, J. W., Katoh, A., Baba, K., and Fujii, T., 2008. A mathematical model for the formation and dissociation of methane hydrates in the marine environment. Journal of Geophysical Research, 113, 1–32, doi: 10.1029/2006JB004768

14. Geletti, R., and Busetti, M., 2011. A double bottom simulating reflector in the western Ross Sea, Antarctica. Journal of Geophysical Research 116, 15p, doi: 10.1029/2010JB007864

15. Grevemeyer, I., and Villinger, H., 2001. Gas hydrate stability and the assessment of heat flow through continental margins. Geophysical Journal International, 145, 647–660, doi: 10.1046/j.0956-540x.2001.01404.x

16. Haacke, R.R., Westbrook, G.K., and Hyndman, R.D., 2007. Gas hydrate, fluid flow and free gas: Formation of the bottom-simulating reflector. Earth and Planetary Science Letters 261, 407-420, doi: 10.1016/j.epsl.2007.07.008

17. Heritier, F.E., Lossel, P., and Wathne, E., 1979. Frigg Field – large submarine-fan trap in lower Eocene rocks of the North Sea Viking Graben. AAPG Bulletin, v. 63/11, 1999-2020.

18. Hornbach, M. J., Saffer, D. M., and Holbrook, W. S., 2004. Critically pressured free-gas reservoirs below gas-hydrate provinces. Nature, 427, 142–144, doi: 10.1038/nature02172

19. Hyndman, R. D., and Davis, E. E., 1992. A mechanism for the formation of methane hydrate and seafloor bottom-simulating reflectors by vertical fluid expulsion. Journal of Geophysical Research: Solid Earth, 97, 7025-7041, doi: 10.1029/91JB03061

20. Hyndman, R. D., Foucher, J.-P., Yamano, M., and Fisher, A., 1992. Deep sea bottom-simulating-reflectors: calibration of the base of the hydrate stability field as used for heat flow estimates. Earth and Planetary Science Letters, 109(3), 289–301.

21. Judd, A., and Hovland, M., 2007. Seabed Fluid Flow: The impact on geology, biology and the marine environment. Cambridge University Press, Cambridge.

22. Karstens, J., and Berndt, C., 2015. Seismic chimneys in the Southern Viking Graben – Implications for palaeo fluid migration and overpressure evolution. Earth and Planetary Science Letters, 412, 88–100, doi: 10.1016/j.epsl.2014.12.017

23. Koch, S., Berndt, C., Bialas, J., Haeckel, M., Crutchley, G. J., and Papenberg, C., 2015. Gas-controlled seafloor doming. Geology, 43, 571–57, doi: 10.1130/G36596.1

24. Kossel, E., Bigalke, N., Pinero, E., and Haeckel, M., 2013. The SUGAR Toolbox – A library of numerical algorithms and data for modelling of gas hydrate systems and marine environments. GEOMAR Report Nr. 8, 160 pp, doi: 10.3289/geomar_rep_ns_8_2013

25. Kvenvolden, K. A., 1995. A review of the geochemistry of methane in natural gas hydrate. Organic Geochemistry, 23, 997–1008, doi: 10.1016/0146-6380(96)00002-2

26. Lericolais, G., Bulois, C., Gillet, H., and Guichard, F., 2009. High frequency sea level fluctuations recorded in the Black Sea since the LGM. Global and Planetary Change, 66(1-2), 65–75, doi: 10.1016/j.gloplacha.2008.03.010

27. Lericolais, G., Bourget, J., Popescu, I., Jermannaud, P., Mulder, T., Jorry, S., and Panin, N., 2013. Late Quaternary deep-sea sedimentation in the western Black Sea: New insights from recent coring and seismic data in the deep basin. Global and Planetary Change 103, 232-247, doi: 10.1016/j.gloplacha.2012.05.002

28. Lüdmann, T., Wong, H., Konerding, P., Zillmer, M., Petersen, C. J., and Flüh, E., 2004. Heat flow and quantity of methane deduced from a gas hydrate field in the vicinity of the Dnieper Canyon, northwestern Black Sea. Geo-Marine Letters, 24(3). 182-193. http://doi.org/10.1007/s00367-004-0169-y

29. Manheim, F. T., and Schug, D. M., 1978. Interstitial waters of Black Sea cores. Initial Reports of the Deep Sea Drilling Project 42 Part 2, 637 – 651.

30. Muratov, M.V., Neprochnox, Y.P., Ross, D.A., and Trimonis, E.S., 1978. Basic features of the Black Sea late Cenozoic history based on results of deep-sea drilling. Initial Reports of the Deep Sea Drilling Project 42 Part 2, 1141 – 1148.

31. Naudts, L., Greinert, J., Artemov, Y. G., Staelens, P., Poort, J., Van Rensbergen, P., and De Batist, M., 2006. Geological and morphological setting of 2778 methane seeps in the Dnepr paleo-delta, northwestern Black Sea. Marine Geology, 227, 177–199, doi: 10.1016/j.margeo.2005.10.005

32. Netzeband, G.L., Hübscher, C.P., Gajewski, D., Grobys, J.W.G., and Bialas, J., 2005. Seismic velocities from the Yaquina forearc basin off Peru: evidence for free gas within the gas hydrate stability zone. International Journal of Earth Sciences 94, 420-432, doi: 10.1007/s00531-005-0483-2

33. Özsoy, E., and Ünlüata, Ü., 1997. Oceanography of the Black Sea: a review of some recent results. Earth-Science Reviews, 42, 231–272.

34. Poort, J., Vassilev, A., and Dimitrov, L., 2005. Did postglacial catastrophic flooding trigger massive changes in the Black Sea gas hydrate reservoir? Terra Nova, 17, 135–140, doi: 10.1111/j.1365-3121.2005.00599.x

35. Popescu, I., Lericolais, G., Panin, N., Wong, H.K., and Droz, L., 2001. Late Quaternary channel avulsions on the Danube deep-sea fan. Marine Geology 179, 25-37.

36. Popescu, I., De Batist, M., Lericolais, G., Nouzé, H., Poort, J., Panin, N., Versteeg, W., and Gillet, H., 2006. Multiple bottom-simulating reflections in the Black Sea: Potential proxies of past climate conditions. Marine Geology 227, 163-176, doi: 10.1016/j.margeo.2005.12.006

37. Posewang, J., and Mienert, J., 1999. The enigma of double BSRs: indicators for changes in the hydrate stability field? Geo-Marine Letters 19, 157-163.

38. Römer, M., Sahling, H., Pape, T., Bahr, A., Feseker, T., Wintersteller, P., and Bohrmann, G., 2012. Geological control and magnitude of methane ebullition from a high-flux seep area in the Black Sea—the Kerch seep area. Marine Geology, 319-322, 57–74, doi: 10.1016/j.margeo.2012.07.005

39. Ryan, W. B. F., Pitman, W. C., III, Major, C. O., Shimkus, K., Moskalenko, V., Jones, G. A., Dimitrov, P., Gorür, N., Sakinc, M., and Yüce, H., 1997. An abrupt drowning of the Black Sea shelf. Marine Geology, 138, 119–126.

40. Sclater, J.G., Jaupart, C., Galson, D., 1980. The heat flow through oceanic and continental crust and the heat loss of the earth. Reviews of Geophysics and Space Physics 18, 269-311.

41. Shipley, T. H., Houston, M. H., and Buffler, R. T., 1979. Seismic evidence for widespread occurrence of possible gas-hydrate horizons on continental slopes and rises. Am. Assoc. Petroleum Geol. Bull. 63, 2204-2213.

42. Sloan, E.D., 1998. Clathrate hydrates of natural gases. Marcel Dekker, New York.

43. Soulet, G., Delaygue, G., and Vallet-Coulomb, C., 2010. Glacial hydrologic conditions in the Black Sea reconstructed using geochemical pore water profiles. Earth and Planetary Science Letters, doi: 10.1016/j.epsl.2010.04.045

44. Tacket, J., and Puckette, J., 2012. Lithologic controls of pressure distribution in sedimentary basins. Search and Discovery Article #40898, AAPG.

45. Tinivella, U., and Guistiniani, M., 2013. Variations in BSR depth due to gas hydrate stability versus pore pressure. Global and Planetary Change 100, 119-128, doi: 10.1016/j.gloplacha.2012.10.012

46. Vassilev, A., and Dimitrov, L., 2002. Spatial and quantity evaluation of the Black Sea gas hydrates. Russ Geol Geophys, 43, 672–684.

47. Wallmann, K., Pinero, E., Burwicz, E. B., Haeckel, M., Hensen, C., Dale, A., and Ruepke, L., 2012. The Global Inventory of Methane Hydrate in Marine Sediments: A Theoretical Approach. Energies, 5(12), 2449–2498, doi: 10.3390/en5072449

48. Winguth, C., Wong, H.K., Panin, N., Dinu, C., Georescu, P., Ungureanu, G., Krugliakov, V.V., and Podshuveit, V., 2000. Upper Quaternary water level history and sedimentation in the northwestern Black Sea. Marine Geology 167, 127-146, doi: 10.1016/S0025-3227(00)00024-4

49. Wong, H.K., Winguth, C., Panin, N., Dinu, C., Wollschläger, M., Georgescu, P., Ungereanu, G., Krugliakov, V.V., and Podshuveit, V., 1997. The Danube and Dniepr fans, morphostructure and evolution. GeoEcoMarina 2, 77-102.

50. Wood, W.T., Gettrust, J.F., Chapman, N.R., Spence, G.D., and Hyndman, R.D., 2002. Decreased stability of methane hydrates in marine sediments owing to phase-boundary roughness. Nature 420, 656 – 660, doi: 10.1038/nature01261